

High-Field-Side RF Injection for Excitation of Electron Bernstein Waves^{*)}

Ryota YONEDA, Kazuaki HANADA¹⁾, Hatem EISERAFY,
Nicola BERTELLI²⁾ and Masayuki ONO²⁾

Interdisciplinary Graduate School of Engineering Sciences, Kyushu University, Kasuga 816-8580, Japan

¹⁾*Research Institute for Applied Mechanics, Kyushu University, Kasuga 816-8580, Japan*

²⁾*Princeton Plasma Physics Laboratory, Princeton, New Jersey 08543, USA*

(Received 27 December 2017 / Accepted 2 July 2018)

An evaluation of high-field-side (HFS) X-mode injection for the electron-Bernstein-wave (EBW) scenario is performed using the GENRAY ray-tracing code. In the early stage of low-density plasma start-up, when the electron cyclotron resonance and upper hybrid resonance layers are close to each other, efficient and localized heating by the EBW is attainable. We show that, when the electron density rises, the HFS scenario spontaneously shifts to current drive with successful electron heating. This shift can be explained as a change in heating mechanism from collisional to electron cyclotron damping. Also, we discuss a possible O-X-B scenario to continue the plasma current drive beyond the formation of an over-dense plasma.

© 2018 The Japan Society of Plasma Science and Nuclear Fusion Research

Keywords: electron Bernstein wave, electron cyclotron, high field side, plasma heating and current drive, mode conversion

DOI: 10.1585/pfr.13.3402115

1. Introduction

Non-inductive current drive is one of the crucial topics in regard to spherical tokamak (ST), where space for the central solenoid is technically limited [1]. Radio-frequency (RF) waves in the range of the electron cyclotron frequency are commonly used in heating and current drive in STs [2–5]. In the initial phase of plasma build-up, the first pass absorption at the electron cyclotron resonance (ECR) layer is very small because the electron temperature T_e and density n_e are low, and multiple reflections of RF waves inside the vessel enable RF-induced breakdown [6–8].

The excitation of electron Bernstein waves (EBWs) could result in highly efficient heating of magnetized plasmas [9–12]. The significance of the EBW often arises in the context of over-dense plasma, where the electron plasma frequency ω_{pe} is larger than the electron cyclotron frequency Ω_{ce} ($\omega_{pe}/\Omega_{ce} > 1$); therefore, the accessibility of electromagnetic electron cyclotron waves to the ECR layer disappears. In contrast, the electrostatic EBW may propagate in the over-dense regime and be strongly damped near the ECR layers. Also, in the initial discharge phase where we have lower T_e , efficient collisional damping of the EBW is expected because the group velocity of the EBW is comparable with electron thermal velocity. There are several ways to excite EBWs in a tokamak configuration but, in the initial low-density phase, where the electron

density is less than the cutoff density, only the extraordinary mode (X-mode) injection from the high field side (HFS) is available. The other methods (O-X-B and X-X-B) require an over-dense regime. Here, O and B stand for ordinary mode and EBW, respectively. We expect the X-mode launched from the HFS to fully convert to the EBW in the upper hybrid resonance (UHR) layer [13]. The difficulty of HFS injection lies in the engineering implementation; a waveguide at the HFS must cross the ECR layer and suppressing RF breakdown inside the waveguide is necessary. In a laboratory test, we demonstrated the transmission of 20-kW RF power through the ECR layer inside a waveguide, which was filled with SF₆ to suppress breakdown.

In this study, we investigated the feasibility of EBWs in the low-density-phase for the initial tokamak plasma start-up by RF injection from the HFS of the tokamak configuration. Adopting EBWs in the low-density regime has a significant advantage when the ECRH is less efficient. The calculation of wave propagation and absorption was performed using GENRAY ray-tracing code [14, 15]. The magnetic configuration used here is based on the experimental results of the QUEST spherical tokamak [16]. The RF frequency and power are set at 8.2 GHz and 50 kW to model the experimental set-up of the 8.2-GHz HFS X-mode in QUEST.

2. HFS Injection Scenarios for EBWs

First, we confirmed the conditions right after breakdown when T_e and n_e are very low. Note that the O-

author's e-mail: yoneda@triam.kyushu-u.ac.jp

^{*)} This article is based on the presentation at the 26th International Toki Conference (ITC26).

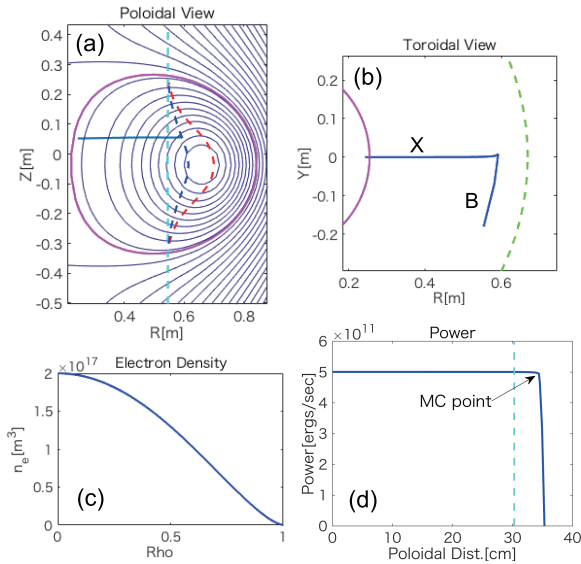


Fig. 1 Low-density regime: (a) Poloidal view of ray-tracing. Light blue dotted line is the 1st ECR, red dotted line is the Rcutoff, blue dotted line is the UHR and magenta line is the lastclosed flux surface. The 1st ECR and UHR are located close to each other; (b) Toroidal view of ray-tracing. Green dotted line is the magnetic axis. The X-mode is converted to EBW at UHR and it starts to propagate in parallel direction; (c) Density n_e profile. Rho is the minor radius defined by r/a ; (d) RF power absorption with poloidal projection of ray. Light blue dotted line is the 1st ECR, where the X-mode passes through. The X-B mode conversion (MC) point is also indicated.

X-B mode conversion cannot be used at this low density because there is no O-mode cutoff. Ray-tracing results by GENRAY are shown in Fig. 1. A spatially uniform $T_e = 5 \text{ eV}$ and a n_e of $n_e(0) = 2 \times 10^{17} \text{ m}^{-3}$ at the center that is approximately 25% of the cutoff density ($n_{e,\text{cut}} = 8.3 \times 10^{17} \text{ m}^{-3}$) for 8.2 GHz electromagnetic waves, are set up. To evaluate collisional damping, Z_{eff} is set to 3 for all conditions presented in this study. The coefficient of absorption associated with electron collisions with ions $\alpha_{\text{cl}} [\text{m}^{-1}]$ is expressed as

$$\alpha_{\text{cl}} = 2v_{\text{ei}}/v_{\text{g}},$$

$$v_{\text{ei}} = 9.17 \times 10^{-17} n_e Z_{\text{eff}} \ln \Lambda / T_e^{3/2} \quad (T_e \text{ in keV}),$$

where v_{ei} is the electron-ion collision rate, v_{g} the group velocity of the waves, and $\ln \Lambda$ the Coulomb logarithm. In GENRAY, the calculation of α_{cl} is taken along the ray's propagation path to estimate collisional damping. Because the ECR and UHR gap is small [Fig. 1 (a)], we can expect efficient and localized absorption of the EBWs. GENRAY can distinguish the damping mechanisms of the cyclotron and collisional absorptions that contribute to both damping effects and are comparable in this configuration with low n_e and T_e . For cyclotron damping absorption, the Doppler-shifted resonance is included to evaluate the evolution of the parallel refractive index N_{\parallel} for EBWs [17].

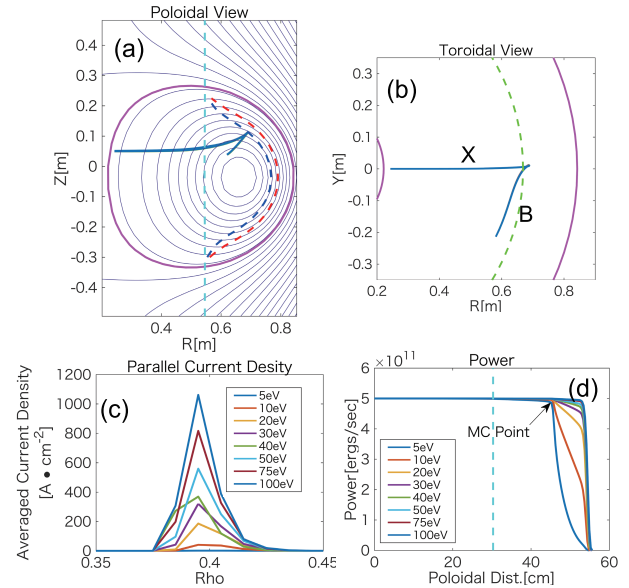


Fig. 2 Medium-density regime: (a) Poloidal view of ray-tracing, (b) Toroidal view of ray-tracing (for different T_e , ray trajectories are almost the same), (c) Parallel current density driven by cyclotron damping with different T_e (note that the horizontal axis is zoomed in), and (d) RF power absorption with the poloidal projection of the rays for different T_e .

In Fig. 1 (d), the power absorption of the perpendicular X-mode at the 1st ECR is included but is negligible with low T_e ; the EBW is rapidly damped right after the X-B mode conversion. An important point to note is that the X-mode should be launched off-mid-plane to control the current drive direction [11].

Second, we consider the case when n_e increases but remains below the over-dense regime. To explore the effect of T_e , we varied the value of T_e from 5 eV to 100 eV. Figure 2 shows results for center $n_e(0)$ set to $8.0 \times 10^{17} \text{ m}^{-3}$ and T_e is spatially homogeneous. The current density and power absorption profiles under cyclotron damping were plotted [Figs. 2 (c) and (d)]. The contribution of cyclotron damping clearly dominates relative to collisional damping at higher T_e . Figure 2(d) shows the difference in the damping mechanism, in which plasma fully absorbs the injected RF power. At $T_e = 5 \text{ eV}$, collisional damping of the EBW is dominant and the absorption is localized near the UHR layer. In contrast, as T_e increases, the location of absorption moves closer to the ECR layer as expected for cyclotron damping. As the toroidally propagating EBW [Fig. 2 (b)] can transfer wave momentum to excite the driven current I_{cd} , the current density increases with higher T_e [Fig. 2 (c)]. GENRAY evaluates the current drive generated by the injection of electron cyclotron waves. In Fig. 3, the dependence of I_{cd} with T_e is shown. With 50-kW injection, it suggests that $I_{\text{cd}} \sim 20 \text{ kA}$ is almost possible. Moreover, cyclotron damping becomes dominant when $T_e \geq 15 \text{ eV}$. If T_e increases successfully with

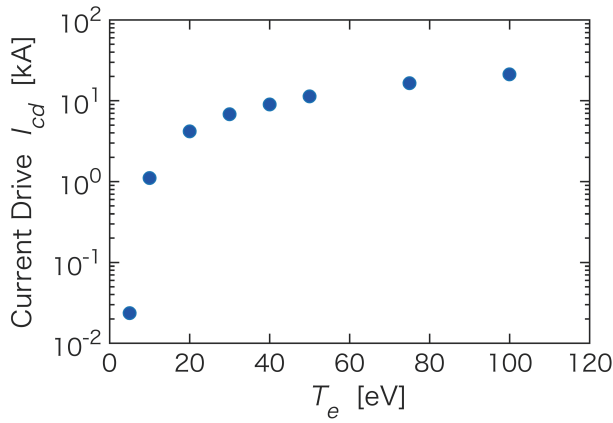


Fig. 3 Dependence of the net current drive I_{cd} on T_e obtained using GENRAY.

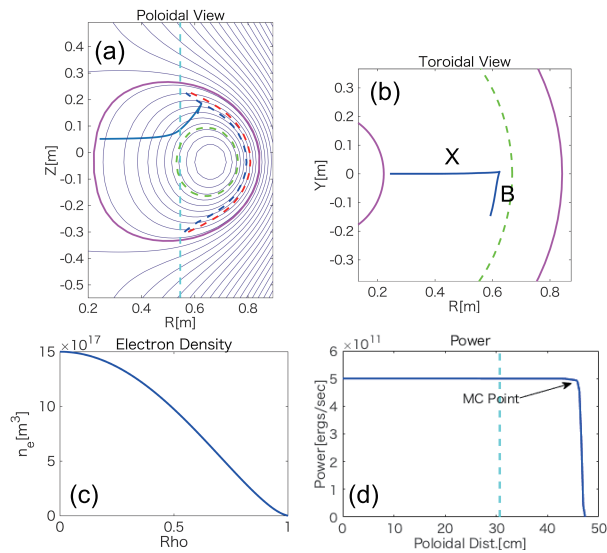


Fig. 4 Over-dense regime: (a) Poloidal view of ray-tracing. Green dotted line is O-cutoff, (b) Toroidal view of ray-tracing, (c) n_e profile, and (d) RF power absorption with the poloidal projection of the ray.

the injected RF power, then we can say that from the calculation the HFS X-mode scenario automatically shifts to EBW current drive from heating.

Third, we examined the HFS X-mode scenario in the over-dense phase. In Fig. 4, we set n_e at the center $n_e(0) = 1.5 \times 10^{18} \text{ m}^{-3}$, which is about twice the cutoff density ($n_{e_cut} = 8.3 \times 10^{17} \text{ m}^{-3}$) for 8.2 GHz. A temperature of $T_e = 50 \text{ eV}$ is assumed to be spatially uniform. With increased n_e , the X-mode starts to bend. In the calculations, the accessibility to the UHR layer disappears when $n_e(0) \sim 2.0 \times 10^{18} \text{ m}^{-3}$. Ray-tracing has been demonstrated with a single ray but does not take into account multiple reflections. Even though the accessibility disappears for the first pass, the reflected electromagnetic waves may still reach the UHR as a X-mode and excite an EBW. The HFS injection scenario has an advantage at this point in that it

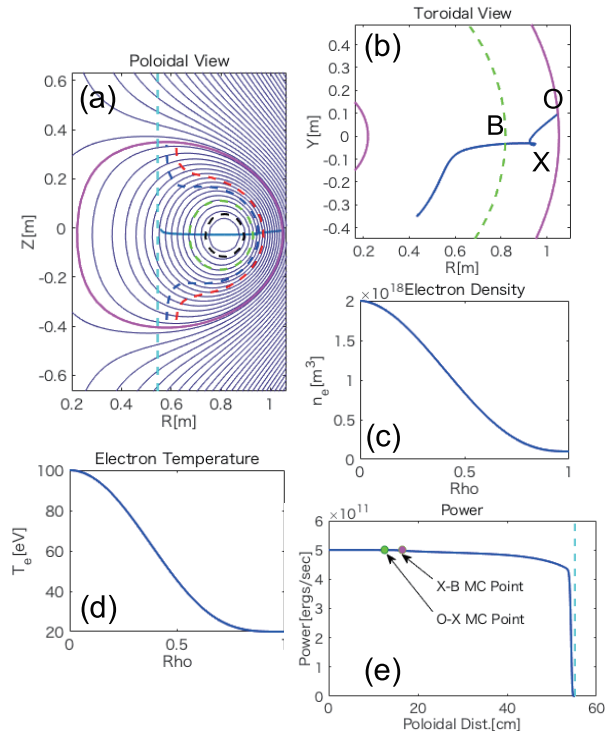


Fig. 5 O-X-B scenario: (a) Poloidal view of ray-tracing. Green dotted line is the O-cutoff and the black dotted line is the Lcutoff, (b) Toroidal view of ray-tracing, (c) n_e profile, (d) T_e profile, and (e) RF power absorption with poloidal projection of the ray. O-X and X-B mode-conversion points are specified.

no longer has to propagate the evanescent layer after reflections at the cutoffs or the vessel walls.

3. LFS Injection Scenarios for EBWs

Next, we evaluated a possible O-X-B mode conversion scenario after the formation of the over-dense plasma. For this scenario, an O-mode launched from the low field side (LHS) must hit an optimized O-X conversion point and then the X-mode excites the EBW at the UHR. GENRAY also can simulate an O-X-B scenario; see Fig. 5. The n_e and T_e profiles [Figs. 5(c) and (d)] are assumed to be Gaussian-like distributions. After X-B conversion, the EBW is gradually absorbed through collisional damping and is strongly damped near the ECR layer. Absorption is localized at the ECR layer but some power is absorbed prior to ECR [Fig. 5(e)]. The net plasma current driven by the EBW excited via the O-X-B mode conversion was evaluated, yielding $I_{cd} = 8.8 \text{ kA}$. This value does not take into account the conversion loss during O-X-B mode conversion. This scenario involves a triplet of resonances and cutoffs and hence its evaluation is more difficult compared with the HFS X-B scenario. In principle, the O-X mode conversion efficiency cannot be calculated directly by ray-tracing. A slight change from the optimum launching for smooth O-X conversion in GENRAY may

also allow an O-X mode conversion with less efficiency. For waves that have a finite width and launched with an arbitrary angle, introducing a full wave calculation is required or a model which can restart the ray-tracing after transmission through the evanescent region to estimate the characteristics of wave propagation including the O-X mode conversion and the absorption [18]. Therefore, the power of the waves launched with a finite width is expected to be reduced to some extent after O-X mode conversion. In contrast, the HFS X-mode scenario has an advantage in that the launched waves can access the UHR without confronting the evanescent region and can be mode converted fully to the EBW even if they have a finite width.

Another possible scenario from LFS is the direct X-B (X-X-B) conversion through the tunneling of the X-mode at the R-cutoff [19, 20]. With this direct X-mode scenario, a precise handling of the launch angle is not required but is necessary for O-X-B; here, the launched RF power should be relatively larger to transport the injected X-mode beyond the R-cutoff because reflections at the R-cutoff are not negligible [19].

4. Summary

In summary, an evaluation of HFS X-mode injection for EBW heating and current drive has been performed using GENRAY. First, in the early stage of start-up, when the ECR and UHR layers are close to each other, efficient and localized heating by EBWs is attainable. Second, for increased n_e , we showed that the HFS scenario spontaneously shifts to current drive as T_e increases. This shift can be explained by the change in heating mechanism from collisional to electron cyclotron damping. Third, we explored the HFS X-mode in the over-dense regime. We also considered a possible O-X-B scenario to continue the

plasma current drive beyond the formation of the over-dense plasma. All ray-tracing results presented are single-ray analyses. To examine realistic experimental conditions, a multiple-ray analysis may be needed.

Acknowledgements

This work was supported by Japan/U.S. Cooperation in Fusion Research and Development in 2016 and 2017. The Author (R.Y.) kindly acknowledges the financial support from Kyushu University Program for Leading Graduate Schools, Advanced Graduate Program in Global Strategy for Green Asia. We thank Richard Haase, Ph.D, from Edanz Group for editing a draft of this manuscript.

- [1] M. Ono and R. Kaita, *Phys. Plasmas* **22**, 040501 (2015).
- [2] H. Idei *et al.*, *Nucl. Fusion* **57**, 126045 (2017).
- [3] T. Yoshinaga *et al.*, *Nucl. Fusion* **47**, 210 (2007).
- [4] M. Ishiguro *et al.*, *Phys. Plasmas* **19**, 062508 (2012).
- [5] S. Tashima *et al.*, *Nucl. Fusion* **54**, 23010 (2014).
- [6] R. Yoneda *et al.*, *Phys. Plasmas* **24**, 062513 (2017).
- [7] D.R. Whaley *et al.*, *Nucl. Fusion* **32**, 757 (1992).
- [8] Y.H. An *et al.*, *Nucl. Fusion* **57**, 016001 (2017).
- [9] A.K. Ram and S.D. Schultz, *Phys. Plasmas* **7**, 4084 (2000).
- [10] A.K. Ram *et al.*, *Phys. Plasmas* **9**, 409 (2002).
- [11] C.B. Forest *et al.*, *Phys. Plasmas* **7**, 1352, (2000).
- [12] V.F. Shevchenko *et al.*, *Nucl. Fusion* **50**, 22004 (2010).
- [13] T. Maekawa *et al.*, *Phys. Rev. Lett.* **86**, 3783 (2001).
- [14] A.P. Smirnov and R.W. Harvey, *Bull. Am. Phys. Soc.* **40**, 1837, abstract 8p35 (1995).
- [15] E. Mazzucato *et al.*, *Phys. Fluids* **30**, 3745 (1987).
- [16] K. Hanada *et al.*, *Nucl. Fusion* **57**, 126061 (2017).
- [17] C.B. Forest *et al.*, *Nucl. Fusion* **41**, 619 (2001).
- [18] H. Igami *et al.*, *Plasma Fusion Res.* **11**, 2403098 (2016).
- [19] M. Ali Asgarian *et al.*, *Phys. Plasmas* **21**, 092516 (2014).
- [20] J.G. Jo *et al.*, *Phys. Plasmas* **24**, 012103 (2017).